



HAL
open science

Development and modeling of filled silicone architected membranes

Marie Rebouah, Grégory Chagnon, Denis Favier

► **To cite this version:**

Marie Rebouah, Grégory Chagnon, Denis Favier. Development and modeling of filled silicone architected membranes. *Meccanica*, 2015, 50 (1), pp.11-24. 10.1007/s11012-014-0065-0 . hal-01480381

HAL Id: hal-01480381

<https://hal.science/hal-01480381>

Submitted on 6 Apr 2018

HAL is a multi-disciplinary open access archive for the deposit and dissemination of scientific research documents, whether they are published or not. The documents may come from teaching and research institutions in France or abroad, or from public or private research centers.

L'archive ouverte pluridisciplinaire **HAL**, est destinée au dépôt et à la diffusion de documents scientifiques de niveau recherche, publiés ou non, émanant des établissements d'enseignement et de recherche français ou étrangers, des laboratoires publics ou privés.

Development and modeling of filled silicone architected membranes

M. Rebouah · G. Chagnon · D. Favier

Abstract The main objective of this study is to generate anisotropic membranes stretched in their plane able to endure large deformations. In this perspective, different crenellated membranes were designed with a filled silicone rubber. The aim of this work is to build a constitutive equation which describes the mechanical behavior of such architected membranes, by means of a simple decomposition of the strain energy. Since a filled silicone is used to make the architected membrane, some non linear effects influence also the mechanical behavior of the structure. The main phenomenon is the Mullins effect and must be taken into account in the modeling. An equivalent constitutive equation is built for the architected membrane by taking into account the mechanical behavior of the silicone and the geometrical parameters of the crenellated membrane. Firstly, a constitutive equation is chosen to describe the core of the membrane. Second, this equation is adapted to the behavior of the crenels and thirdly a coupling term describing the interactions between the crenels and the core of the membrane is developed. The implementation of the equivalent constitutive equation into a finite element code is finally validated on experimental data.

Keywords Architected material · Silicone rubber · Stress-softening · Constitutive equation

1 Introduction

Architected materials take an increasingly important place in many applications due to their specificities including mechanical properties [4]. It exists several types of architected materials. For instance, some materials are architected due to their microstructure (grain size for metallic materials, polymer chain design or state of crystallization for example). This strategy operates at scales between 1 nm and 10 μm . Architected materials can also be composed with an association of several materials (also called hybrid material). Other materials can be considered as architected because of their geometry. These architected materials are usually used to build multifunctional materials [1, 3, 5].

[14] developed crenellated membranes with an unfilled silicone rubber. The main advantage of these membranes is that they present an anisotropic behavior without any interface in the material. Indeed, the crenels and their orientations allow to induce and control the anisotropy. The architected membranes can be separated in three parts, the core of the membrane (the central part) and the upper and lower lattices of crenels that are on the external surfaces of the core of the membrane. The silicone used by [14]

M. Rebouah · G. Chagnon (✉) · D. Favier
Université de Grenoble Alpes/CNRS/TIMC-IMAG UMR
5525, 38041 Grenoble, France
e-mail: gregory.chagnon@imag.fr

was perfectly hyperelastic but suffered from bad properties in tearing which makes it difficult to use in real applications. In this study it is chosen to develop the same crenellated membranes, with a filled silicone rubber to improve the resistance of the material. Due to the fillers, the material presents good tearing properties although it shows other phenomena like stress softening or hysteresis.

The goal of this paper is to study the mechanical behavior of such architected membranes when they are stretched in their planes and to develop the associated constitutive equation. A method to develop an equivalent model of the core of the membrane and the crenels is presented. The membrane properties come from the bulk material, i.e. the filled material. Its main properties are to support reversible large deformations and to endure stress softening [6, 16] that induces anisotropy [12]. First, in Sect. 2 the experimental set up and the architected membranes are described. Several tests are performed to highlight the mechanical behavior. In Sect. 3, a theoretical study presents the constitutive equation developed to build the strain energy of the architected membranes. In Sect. 4, the constitutive equations are implemented into a Finite Element (FE) code. A comparison between the FE simulation and a complex experimental test is proposed. Finally, Sect. 5 presents some conclusions and perspectives.

2 Materials and methods

The same filled silicone rubber (RTV3428) is used to manufacture all the architected membranes presented in the paper. This material was already used in previous works and some non linear phenomena as hysteresis, relaxation [11, 21] and induced anisotropy [13] were already studied. As illustrated by [21], the Mullins effect is the prevailing phenomenon so the experimental results focus on the study of this phenomenon. The other phenomena are not considered in a first approach.

2.1 Description of the architected membrane

The architected membranes are manufactured according to the process described by [14], by injection molding to obtain circular architected plane membranes. For that purpose, a specific mold

was used. The mold is composed of two circular crenellated metallic plates of 16 cm diameter, each one of these plates comes lock another holey metallic plate on each side. When the holey plate is locked, there is a space of 1 mm between the two crenellated plates. Besides, the two crenellated plates can be fixed separately in any wished angular position. Thus, any circular architected membrane with different crenels orientations can be molded. Once the injection is done, the mold filled out of silicone is put at 70 °C for 4 hours into an oven to accelerate the vulcanization. Finally, flat membranes ascribed of geometrical motifs (lattices of parallel crenels) on the upper and lower external surfaces are obtained. Due to the geometry of the architected membranes, several coordinate systems have to be defined and are presented in Fig. 1. Two coordinate systems are defined for the two crenels layers. For the first crenel the basis denoted $R_1(\mathbf{E}_1, \mathbf{K}_1, \mathbf{z})$ is defined and for the second crenel the basis denoted $R_2(\mathbf{K}_2, \mathbf{E}_2, \mathbf{z})$. The vector \mathbf{E}_i corresponds to the crenel direction, \mathbf{K}_i is an orthogonal vector in the plane of the membrane, and \mathbf{z} is orthogonal to the plane (\mathbf{x}, \mathbf{y}) of the membrane. It is to note that the architected membranes are characterized by the angle α between the two lattices of the crenels, thus α is the angle defined by the orientations \mathbf{E}_1 and \mathbf{E}_2 . Finally, a global coordinate system is introduced $R(\mathbf{x}, \mathbf{y}, \mathbf{z})$. The vector \mathbf{y} matches the bisector of the orientations of the crenels and \mathbf{x} is an orthogonal vector in the plane of the membrane. For the following the model is defined in the basis R of the architected membrane.

In order to study the influence of the crenel orientations, five different circular architected membranes were molded with the same material and same processing. For each architected membrane, the only parameter that changes is the relative orientation α between the crenels, the geometry of the crenels stays the same. Finally, architected membranes with $\alpha = 0^\circ, 45^\circ, 90^\circ, 135^\circ$ and 180° are manufactured. Tensile rectangular specimens were cut from the circular plate samples along the direction \mathbf{y} (as illustrated in Fig. 1) i.e. along the bisector of the crenels orientations. The initial dimensions of the tensile samples are $L = 60$ mm long, $l = 21$ mm width and $e = 1$ mm thick for the core of the membrane. The crenels on the external surfaces of the membrane are spaced out of 2 mm and the width and thickness of each crenel are 1 mm (cf. Fig. 1).

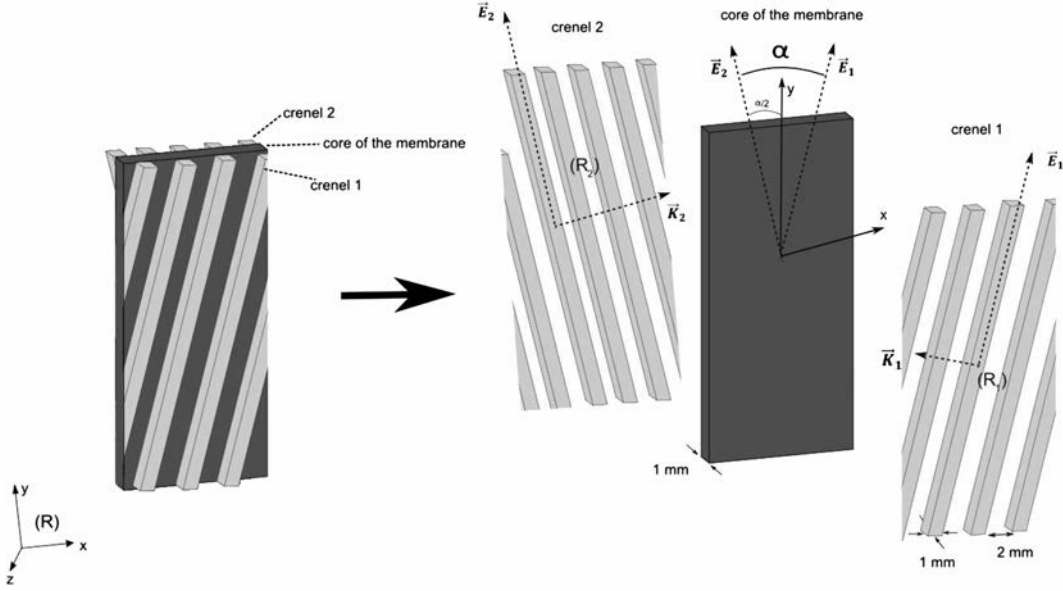


Fig. 1 Geometry of the architected membrane, on the *left* the specimen is presented, on the *right* the specimen is presented in a cut version to highlight the three layers

2.2 Experimental set up

For each architected tensile test sample, a cyclic tensile test along the vector y (corresponding to the bisector of the crenels orientations) was processed. By means of tension device, the samples underwent a cyclic tensile test up at three different elongations λ , where λ represents the current length of the sample over its initial length. The first loading unloading cycle is reached at $\lambda = 1.5$, the second at $\lambda = 2.$, and the third at $\lambda = 2.5$. After these three cycles a reloading at $\lambda = 2.5$ is performed. The measurements are made by means of a 100 N load cell which is synchronized to a stereo-dimensional image correlation (SDIC) system. This technique enables to determine the 3D contour and the in-plane strain fields of the object surface. Then the strain fields of the architected membrane can be studied at any point of the surfaces. The specimens present a periodic structure which has to be repeat at least seven times in the width of the specimen to consider a continuum model. Due to the crenel orientations, the section of the specimens is different for each membrane. Thus, it is proposed to analyze the results using the nominal tension T to have a more realistic comparison for all the samples. The nominal tension is defined as:

$$T = \frac{F}{l_0} \quad (1)$$

where F is the applied force and l_0 the initial width.

2.3 Experimental results

The results of the tensile tests are presented in the Fig. 2 for the five different orientations of crenels. Figure 2a presents the evolution of the transversal elongation λ_x during the tensile test in the REV, which was measured by means of SDIC, in function of the tensile elongation, i.e. λ_y . The solid line represents the theoretical transversal elongation for a tensile test on an incompressible isotropic material and the dashed lines represent the experimental transversal elongation for the membranes with different orientations α . For an orientation of $\alpha = 0^\circ$, the transversal elongation matches perfectly the mechanical behavior of incompressible isotropic material, i.e. $\lambda_x = \frac{1}{\sqrt{\lambda_y}}$. For orientations of $\alpha = 45^\circ$ and $\alpha = 90^\circ$ the curves are overlapping and present a behavior very close to the theoretical behavior of an incompressible isotropic material but with little lower transversal elongations. At the opposite, for $\alpha = 135^\circ$ and 180° , the transversal elongations are largely different from the

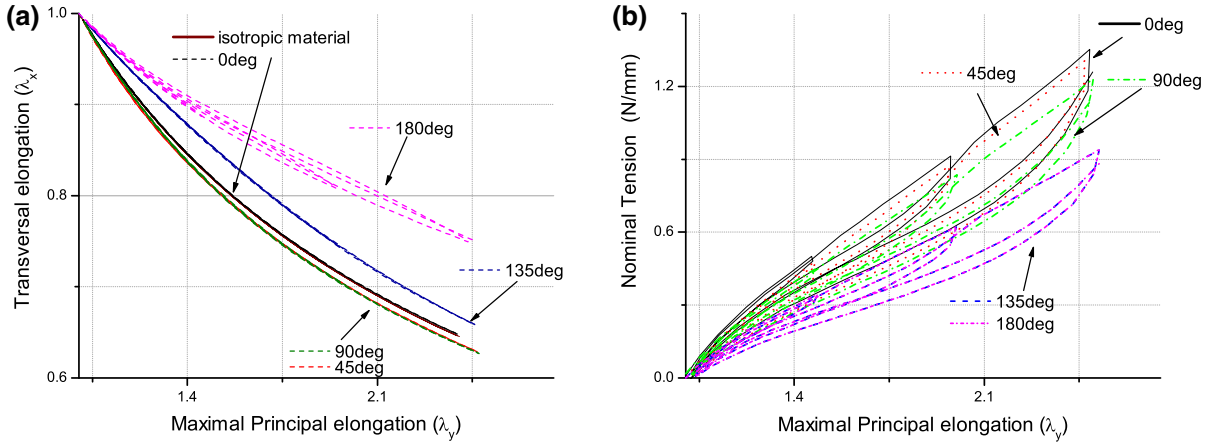


Fig. 2 Evolution of the transversal elongation (a) and nominal tension (b) of the architected membrane for different crenel orientations $\alpha = 0^\circ, 45^\circ, 90^\circ, 135^\circ$ and 180°

incompressible isotropic material. Figure 2b illustrates the evolution of the nominal tension in function of the tensile elongation. It is observed that the orientation α between the crenels strongly influences the tension in the membrane. The lower orientation requires the higher tension to deform the architected membrane. It is to note that few differences are observed for $\alpha = 135^\circ$ and $\alpha = 180^\circ$. The same results were observed by [14] with an unfilled silicone rubber. Nevertheless, compared to [14], the bulk material presents phenomena as hysteresis and Mullins effect that can also be observed for the crenellated membranes. As for the bulk material, it appears that the Mullins effect is important and that in comparison the hysteresis is weaker.

3 Architected filled silicone membrane constitutive equation

3.1 General form

Rubber like materials are described by means of a strain energy density \mathcal{W} . It is proposed to decompose the strain energy function as the sum of the strain energies of the core of the membrane $\mathcal{W}_{\text{core-membrane}}$ and of each crenel $\mathcal{W}_{\text{crenel-1}}$, $\mathcal{W}_{\text{crenel-2}}$ as:

$$\mathcal{W} = \mathcal{W}_{\text{core-membrane}} + \mathcal{W}_{\text{crenel-1}} + \mathcal{W}_{\text{crenel-2}} + \mathcal{W}_{\text{coupling}} \quad (2)$$

Another term $\mathcal{W}_{\text{coupling}}$ is added in order to represent the strain energy density of coupling between the

crenels and the membrane. The strain energy densities should take into account the observed phenomena during experimental tests. It is proposed in a first approach to develop a constitutive equation taking into account only the hyperelasticity and the stress softening of the architected membrane.

3.2 Constitutive equation of the bulk material filled silicone rubber

The filled silicone rubber used in this study presents an induced anisotropy [11, 13]. [19] developed a constitutive equation written with strain invariants to predict the behavior of this material. The strain energy density $\mathcal{W}_{\text{silicone}}$ is additively decomposed into two parts: one that represents the strain energy of the chains linked to other chains \mathcal{W}_{cc} and another part that represents the strain energy of the chains linked to filler \mathcal{W}_{cf} , the total strain energy density is $\mathcal{W}_{\text{silicone}} = \mathcal{W}_{cc} + \mathcal{W}_{cf}$. [19] considered that Mullins effect is mainly due to the presence of fillers. Thus, only \mathcal{W}_{cf} is evolving with the stress softening. \mathcal{W}_{cf} is represented by a microsphere model that can record the deformation history of the material. The 42 spatial initial directions $\mathbf{A}^{(i)}$ proposed by [2] are used. The dilatation in each direction are defined by means of $I_4^{(i)} = \mathbf{A}^{(i)} \cdot \mathbf{C} \mathbf{A}^{(i)}$ where \mathbf{C} is the right Cauchy Green strain tensor, defined as $\mathbf{F} \mathbf{F}^T$, where \mathbf{F} is the deformation gradient. The $\mathbf{A}^{(i)}$ directions are transformed in $\mathbf{a}^{(i)}$ after a deformation by $\mathbf{a}^{(i)} = \mathbf{F} \mathbf{A}^{(i)}$. Finally, the general form of the strain energy in an incompressible framework is:

$$\mathcal{W}_{\text{silicone}} = \mathcal{W}_{cc}(I_1, I_2) + \sum_{i=1}^{42} \omega^{(i)} \mathcal{F}^{(i)} \mathcal{W}_{cf}^{(i)}(I_4^{(i)}). \quad (3)$$

where I_1, I_2 are the first and second strain invariants of the tensor \mathbf{C} , $\omega^{(i)}$ represents the weight of each direction, $\mathcal{F}^{(i)}$ is the Mullins effect evolution function. The [15] strain energy is chosen for \mathcal{W}_{cc} and the strain energy of each chain $\mathcal{W}_{cf}^{(i)}$ is defined as:

$$\mathcal{W}_{cf}^{(i)} = \frac{K}{2} \ln I_4^{(i)} (I_4^{(i)} - 1) \quad (4)$$

where K is a material parameter. The form was modified compared to [19], as the bundle of RTV3428 material used in this paper presents less stress hardening. The same evolution function as proposed by [19] is used:

$$\mathcal{F}^{(i)} = 1 - \eta \sqrt{\frac{I_{1\max} - I_1}{I_{1\max} - 3} \frac{I_{4\max}^{(i)} - I_4^{(i)}}{I_{4\max}^{(i)} - 1} \frac{I_{4\max}^{(i)}}{I_{4\max}}}^4 \quad (5)$$

where η is a material parameter, $I_{1\max}, I_{4\max}^{(i)}$ and $I_{4\max}$ are respectively the maximum values of $I_1, I_4^{(i)}$ for direction i and $I_4^{(i)}$ for all directions $i = 1 \dots 42$. The evolution function cannot be negative since it is considered that each chain can only endure tension and no compression. The Cauchy stress tensor is then the sum of two terms:

$$\boldsymbol{\sigma}_{\text{silicone}} = \boldsymbol{\sigma}_{cc} + \boldsymbol{\sigma}_{cf} \quad (6)$$

$\boldsymbol{\sigma}_{cc}$ is the part of the Cauchy stress that represents the chains linked to other chains and $\boldsymbol{\sigma}_{cf}$ the part of the Cauchy stress that represents the chains linked to fillers. Finally the stress is written as:

$$\begin{aligned} \boldsymbol{\sigma}_{\text{silicone}} = & -p\mathbf{I} + 2\mathbf{B} \frac{\partial \mathcal{W}_{cc}}{\partial I_1} + 2(I_1 \mathbf{B} - \mathbf{B}^2) \frac{\partial \mathcal{W}_{cc}}{\partial I_2} \\ & + 2 \sum_{i=1}^{42} \omega^{(i)} \mathcal{F}^{(i)} \frac{\partial \mathcal{W}_{cf}^{(i)}}{\partial I_4^{(i)}} \mathbf{F}(\mathbf{A}^{(i)} \otimes \mathbf{A}^{(i)}) \mathbf{F}^T \end{aligned} \quad (7)$$

3.3 Strain energy of the core of the membrane

The core of the membrane is the central part of the architected membrane and can be described as the bulk material. Thus, this part of the structure is simply represented by the constitutive equation given by

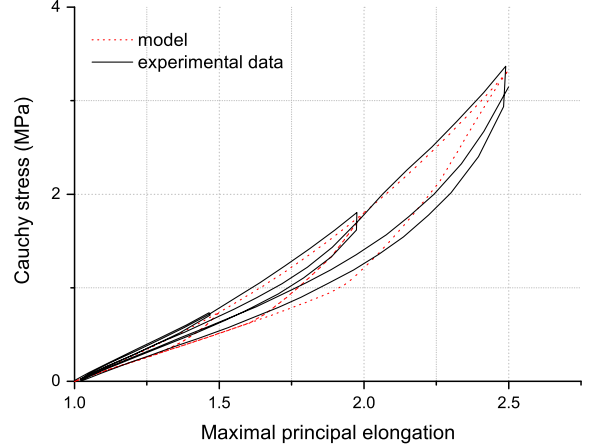


Fig. 3 Comparison of the model and experimental data for the bulk material

Eq. (7). The model is fitted on the bulk material. Figure 3 presents a comparison between the simulation of the model and a tensile cyclic test performed on the filled silicone rubber. The model parameters are: $C_1 = 0.065$ MPa, $C_2 = 0.045$ MPa, $\eta = 9$, $K = 0.27$ MPa. The first load is well described. Some little errors are observed for the second loads but the fit is quite good.

3.4 Strain energy of the crenels

The crenels are processed with the same material as the core of the membrane, so the mechanical characteristics are the same. During the deformation of the membrane, it is considered that crenels are only submitted to tension-compression loading. It is estimated that there is no flexion in the crenels so they are modeled as bars. To determine the stress of each crenel, it is proposed to write the Eq. (7) in term of unidirectional components to represent the uniaxial extension undergone by the crenels. That means that $\boldsymbol{\sigma}_{cf}$ should be described only according to the elongation in the direction \mathbf{E}_k , where k represents either the crenel 1 or the crenel 2. Thus, the behavior of each crenel can be modeled only by means of the fourth invariant $I_{4c}^{(k)}$ corresponding to the direction \mathbf{E}_k , $I_{4c}^{(k)}$ is defined as

$$I_{4c}^{(k)} = \mathbf{E}_k \cdot \mathbf{C} \mathbf{E}_k \quad (8)$$

λ_{E_k} represents the elongation in the direction \mathbf{E}_k . Thus the strain energy of each crenel depends only on the fourth invariant:

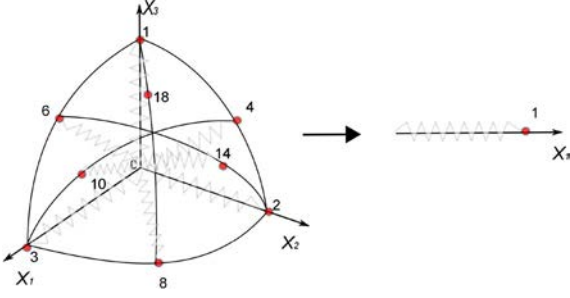


Fig. 4 Representation of a eighth of the 42 directions of Bazant and Oh; replacement of these directions by only one direction for tensile test adapted to one direction for the crenel

$$\mathcal{W}_{\text{crenel-k}} = \mathcal{W}(I_{4c}^{(k)}) \quad (9)$$

The loading state in the crenel can be expressed by the right Cauchy-Green strain tensor $\mathbf{C}_c^{(k)}$ written in the basis \mathbf{R}_k as:

$$\mathbf{C}_c^{(k)} = \begin{pmatrix} \lambda_{\mathbf{E}_k}^2 & 0 & 0 \\ 0 & 1 & 0 \\ 0 & 0 & 1 \end{pmatrix}_{\mathbf{R}_k} \quad (10)$$

As a consequence, the first and second invariants can be expressed in function of $I_{4c}^{(k)}$:

$$I_{c1}^{(k)} = I_{4c}^{(k)} + \frac{2}{\sqrt{I_{4c}^{(k)}}} \quad (11)$$

$$I_{c2}^{(k)} = \frac{1}{2} \left((I_{c1}^{(k)})^2 - \left((I_{4c}^{(k)})^2 + \frac{2}{I_{4c}^{(k)}} \right) \right) \quad (12)$$

The term σ_{cf} in Eq. (7) should be modified in order to be expressed only by means of $I_{4c}^{(k)}$. The objective is to replace the 42 directions by 1 with a new weight $\omega_c^{(i)}$ as illustrated in Fig. 4. First, it is necessary to focus on the first loading curve where the evolution functions $\mathcal{F}^{(i)}$ do not evolve and stay equal to 1. To evaluate the new value of $\omega_c^{(i)}$ noted $\tilde{\omega}$ in the direction \mathbf{E}_k a comparison of the stress σ_{cf} with 42 directions

$$\sigma_{cf} = 2 \sum_{i=1}^{42} \omega_c^{(i)} \mathcal{F}^{(i)} \frac{\partial W_{cf}}{\partial I_4} \mathbf{F} \mathbf{A}^{(i)} \otimes \mathbf{A}^{(i)} \mathbf{F}^T. \quad (13)$$

and with only the \mathbf{E}_k direction is done.

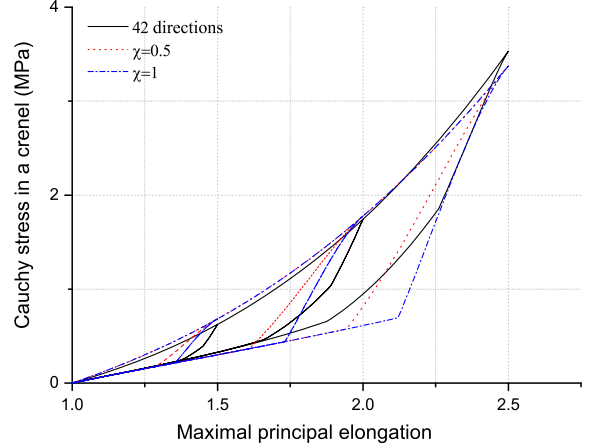


Fig. 5 Cauchy stress for the directional part of the Cauchy stress with 1 direction for $\tilde{\omega} = 0.21$ and $\chi = 0.5$ or $\chi = 1$, and with 42 directions

$$\sigma_{cf-\text{crenel}} = 2\tilde{\omega} \mathcal{F}_c^{(k)} \frac{\partial W_{cf}}{\partial I_{4c}^{(k)}} \mathbf{F} \mathbf{E}_k \otimes \mathbf{E}_k \mathbf{F}^T \quad (14)$$

This comparison allows to deduce the value of the weight for one direction. A value of $\tilde{\omega} = 0,21$ is obtained for the first loading curves to coincide as illustrated in Fig. 5. The parameter used for the representation is $K = 1.07$ MPa but the value of $\tilde{\omega}$ is independent of K . In Eq. (14) W_{cf} is the strain energy for only one direction, i.e. for a crenel, which is identical as the strain energy of the core of the membrane given in Eq. (4).

For the second loading curves, the evolution function $\mathcal{F}^{(i)}$ must be considered. It was described as the product of three terms (cf Eq. (5)). The third term of the product is useless since with only one direction $I_{4\text{max}}^{(k)} = I_{4\text{max}}$, there is no influence of the other directions on the considered one. In tension, the first invariant can be expressed by means of the fourth invariant (cf. Eq. (11)), that means that I_{1c} and I_{4c} are no longer independent variables. Thus the evolution function can only be expressed by way of $I_{4c}^{(k)}$ or $I_{1c}^{(k)}$. It is chosen to express it in function of $I_{4c}^{(k)}$. The evolution function is adapted as:

$$\mathcal{F}_c^{(k)} = 1 - \eta \chi \left(\frac{I_{4c\text{max}}^{(k)} - I_{4c}^{(k)}}{I_{4c\text{max}}^{(k)} - 1} \right)^2 \quad (15)$$

A new parameter χ is introduced to represent the transformation of 42 directions to 1. Figure 5

highlights the role of the intensity χ of the crenels evolution function for a value of $K = 1.07$ MPa and $\eta = 9$. χ has an important role in the form of the second loading curve. It must be a value of 0.5 to limit important slope discontinuities and to represent a behavior closer to the microsphere formulation. As for $\tilde{\omega}$, the determination of χ is independent of the value of the material parameter K and η . Thus, the strain energy of the crenel is defined as:

$$\mathcal{W}_{\text{crenel-k}} = \mathcal{W}_{cc}(I_{4c}^{(k)}) + \tilde{\omega}\mathcal{F}_c^{(k)}\mathcal{W}_{cf}(I_{4c}^{(k)}) \quad (16)$$

Finally, the contribution of the crenel in the membrane stress is defined as:

$$\begin{aligned} \boldsymbol{\sigma}_{\text{crenel}(k)} = & \left(2C_1 \left(I_{4c}^{(k)} - \frac{1}{\sqrt{I_{4c}^{(k)}}} \right) \right. \\ & \left. + 2C_2 \sqrt{I_{4c}^{(k)}} - \frac{1}{I_{4c}^{(k)}} \right) + 2\tilde{\omega}\mathcal{F}_c \frac{\partial \mathcal{W}_{cf}}{\partial I_{4c}^{(k)}} \mathbf{e}_n^{(k)} \otimes \mathbf{e}_n^{(k)} \end{aligned} \quad (17)$$

where $\mathbf{e}_n^{(k)}$ represents the normed instantaneous direction of the crenels such as $\mathbf{e}^{(k)} = \mathbf{F}\mathbf{E}_k$ and $\mathbf{e}_n^{(k)} = \mathbf{e}^{(k)} / \|\mathbf{e}^{(k)}\|$. To determine the tension, a parameter β must be introduced to quantify the proportion of crenels. In fact the crenels have the same height as the core of the membrane but also recover a third of the surface of the membrane (see Sect. 2), that means that $\beta = \frac{1}{3}$.

3.5 Coupling strain energy

It is proposed to develop this term to take into account the coupling effect between the crenels and the core of the membrane. The coupling strain energy term has to take into account the shear induced by the crenels on the external faces of the core of the membrane, i.e. along the two directions \mathbf{E}_1 and \mathbf{E}_2 . The coupling term can be taken into account in different ways. [20] developed a strain energy coupling between orthotropic directions composed by the product of terms isotropic (i.e. I_1) and anisotropic (here $I_{4c}^{(1)}$ and $I_{4c}^{(2)}$). [17], [9] and [18] defined also a constitutive equation by using two other invariants that take into account the shear in the material to model living tissues as heart or annulus fibrosus of the intervertebral disc. In each case, it is proposed to develop a coupling term by

using the eighth and ninth invariants. This approach is considered here:

$$\mathcal{W}_{\text{coupling}} = \mathcal{W}(I_8, I_9) \quad (18)$$

By adaptation of invariants developed by [22], we used:

$$I_8 = \frac{1}{2}(\mathbf{C} : (\mathbf{E}_1 \otimes \mathbf{E}_2) + \mathbf{C} : (\mathbf{E}_2 \otimes \mathbf{E}_1)) \quad (19)$$

$$I_9 = \mathbf{E}_1 \cdot \mathbf{E}_2 \quad (20)$$

Finally a new strain energy density is proposed:

$$\mathcal{W}_{\text{coupling}} = C_8(\alpha) \int \ln(1 + \text{abs}|I_8 - I_9|) dI_8 \quad (21)$$

where $C_8(\alpha)$ represents a material parameter which depends on the orientation α between the crenels to be adapted to every membrane. It represents the torsion stiffness of the core of the membrane according to the initial orientation of the crenels. The coupling Cauchy stress is deduced:

$$\begin{aligned} \boldsymbol{\sigma}_{\text{coupling}} = & C_8(\alpha) \ln(1 + \text{abs}|I_8 - I_9|) \mathbf{F}(\mathbf{E}_1 \otimes \mathbf{E}_2 \\ & + \mathbf{E}_2 \otimes \mathbf{E}_1) \mathbf{F}^T \end{aligned} \quad (22)$$

A quadratic evolution of the parameter with the angle is chosen:

$$C_8(\alpha) = a\alpha^2 \quad (23)$$

where a is a material parameter.

4 Numerical study

The equivalent model, i.e. Eqs. (7–17–22), was implemented into a Finite Element (FE) code (Abaqus 2002) via an UMAT. Details about implementation can be read in [8, 10] and [19]. To validate the model, it is proposed to compare FE simulations to the experimental data of the architected membranes. The equivalent model simplifies the FE calculus by not representing the details of the geometry of the crenellated membrane. Indeed the crenels add a lot of complexity and increase the number of needed elements in the meshes, so by means of the equivalent model it is now possible to sketch a simple geometry (a rectangular plate) and to deduce the behavior of real crenellated plate.

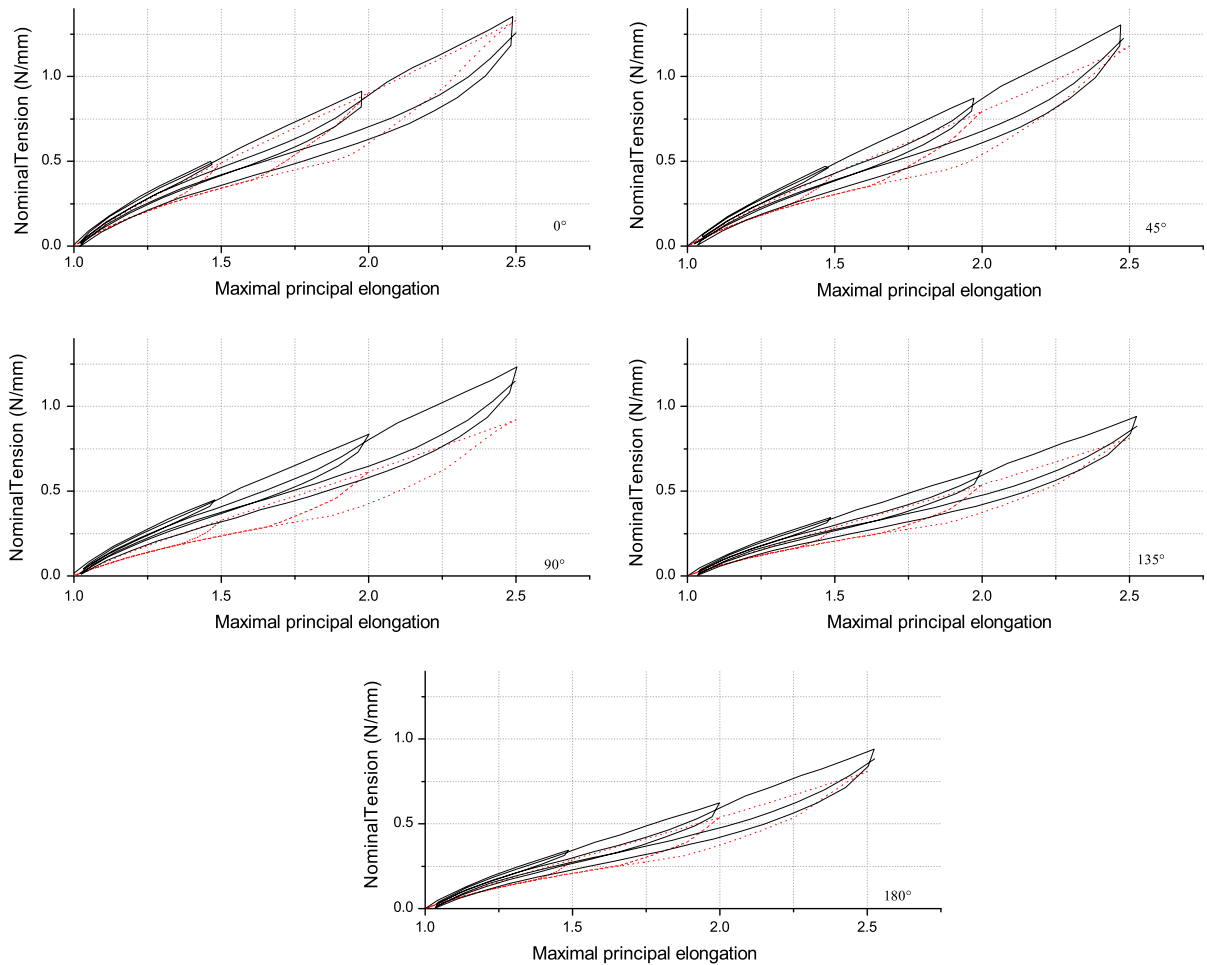


Fig. 6 Comparison of experimental tests (*black full lines*) and the model (*red dotted lines*) of architected membranes for different orientations of the crenels neglecting the shear between the crenels and the core of the membrane. (Color figure online)

4.1 Validation of the model with experimental data without coupling

According to the experimental results presented in the first part, a comparison of the analytical simulations of the equivalent model is realized for each angle $\alpha = 0^\circ, 45^\circ, 90^\circ, 135^\circ$ and 180° . The results are presented in Fig. 6. The values of the mechanical parameters used for the simulations are those of the bulk material and are the same as presented in Sect. 3.3. In a first approach, the coupling term is not taken into account. It is observed that for $\alpha = 0^\circ$ and $\alpha = 180^\circ$ a good match between the model and the experimental results is obtained. Nevertheless for every other values of α the model does not match perfectly with the experimental data, a little difference is observed for $\alpha = 45^\circ$ and

$\alpha = 135^\circ$ and a more important difference is observed for $\alpha = 90^\circ$. These differences can be explained by the shear stresses between the core of the membrane and the crenels that were neglected in this first approach. As no angle variation are observed for 0 and 180° , there is no shear stress. It explains why the comparisons between experimental data and analytical calculus are much better for these two orientations.

4.2 Validation of the model with experimental data with the coupling term

4.2.1 Tensile tests

In this part, the coupling term is no longer neglected and the results of the analytical simulation are

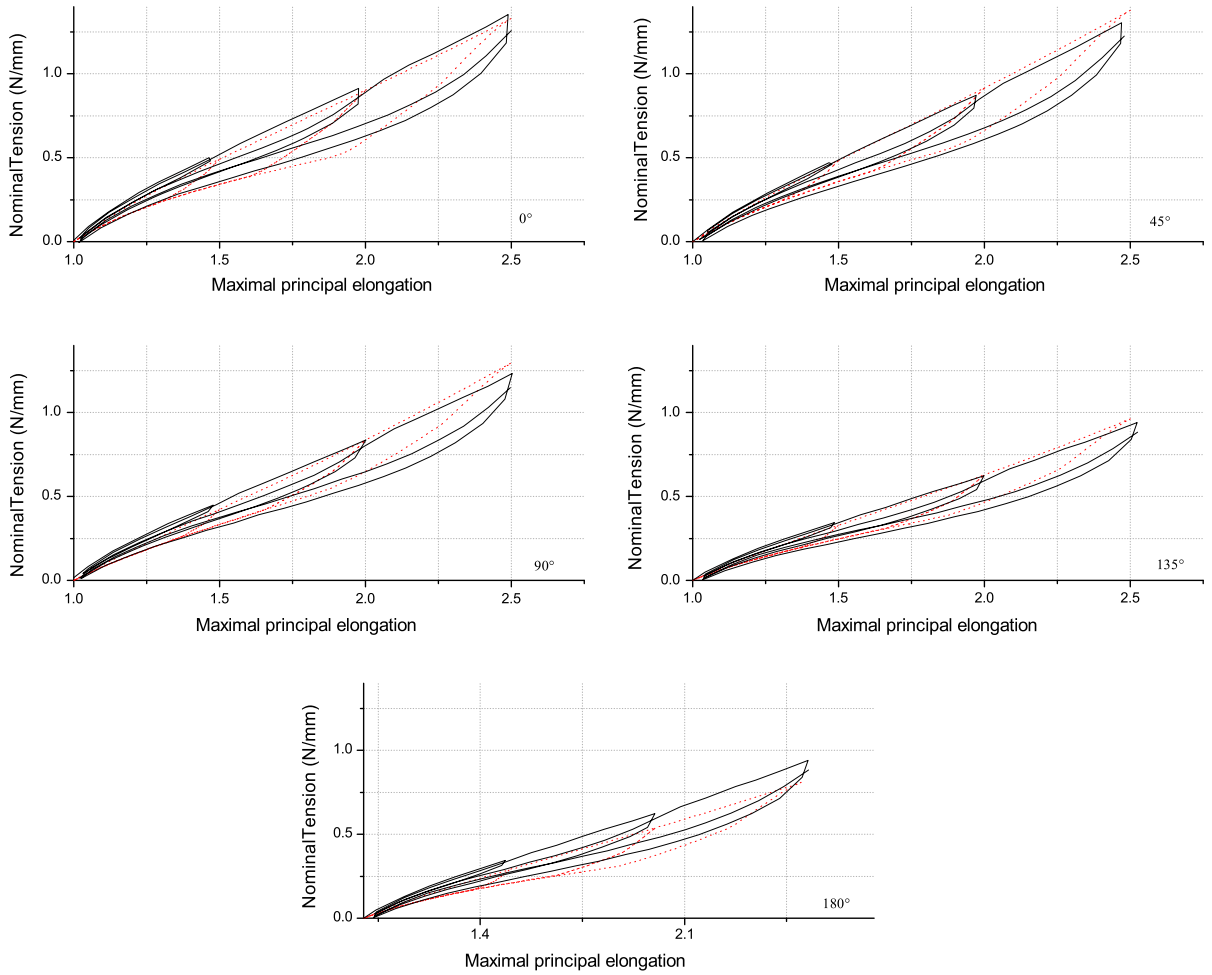


Fig. 7 Comparison of experimental tests (*black full lines*) and the model (*red dotted lines*) of architected membranes for different orientations of the crenels with coupling. (Color figure online)

compared to the experimental data as illustrated in Fig. 7. The only parameter fitted with the equivalent model is the parameter a for the quadratic function (Eq. (23)) which describes the evolution of the coupling term with the angle, a value of $a = 0.028$ MPa is obtained. It is observed that the use of the coupling term allows to have a better matching with the experimental results for each orientation of the crenels. The coupling term permits to take into account the amount of energy used to change the angle between the two crenels. It is important to note that by taking into account the coupling term, good comparison between experimental data and analytical results are obtained. The coupling term is thus a very important term and should not be neglected.

4.2.2 Bulge test

It is proposed to test the constitutive equation in a complex loading FE calculation. A circular architected membrane of 180 mm diameter with an orientation $\alpha = 45^\circ$ is simulated for a numerical bulge test. An experimental cyclic bulge test is also performed on this membrane. The strain state is controlled by pressure, thus the first cycle is reached for a pressure $p = 1.49$ kPa, the second for $p = 3.48$ kPa, the third $p = 5.31$ kPa and finally $p = 7.31$ kPa for the fourth loading. It is proposed to compare the results obtained along a radius of the circular plate. This path is defined to take into account the different biaxial loading states reached during a bulge test. As presented in Fig. 8a,

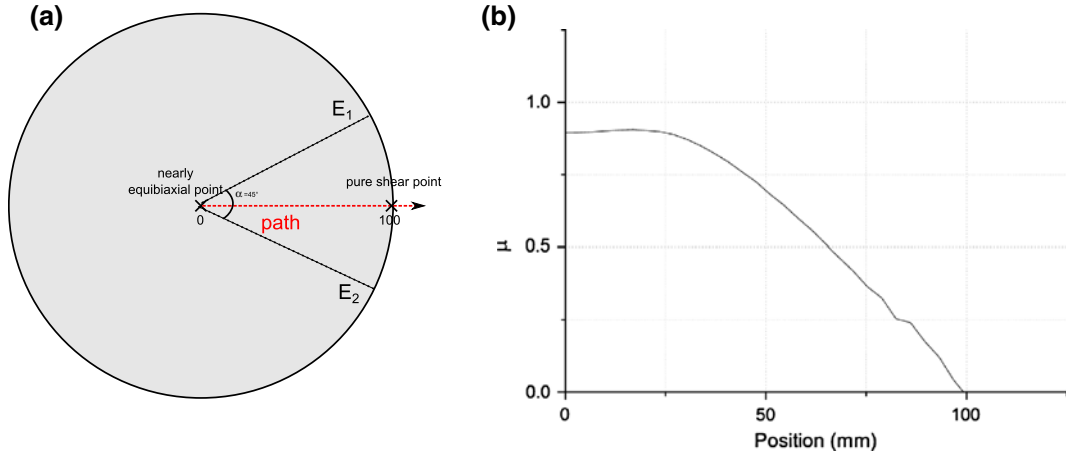


Fig. 8 **a** representation of the studied path on the bulge test [13]. **b** Biaxiality ratio along the path

the start point is the center of the plate which is close to an equibiaxial point (the equibiaxial point is only reached for an isotropic material) and the second point is at the fixing of the plate, it corresponds to pure shear [12]. Figure 8b represents the biaxiality ratio along the path, defined as $\mu = \ln(\lambda_{\min})/\ln(\lambda_{\max})$ (where λ_{\min} and λ_{\max} are the minimum and maximum in-plane principal elongations) for a pressure level $p = 1.49$ kPa. It is observed that the biaxiality ratio varies a lot between the two extremal loading points. Thus, this test permits to verify the robustness of the model on very different biaxial strain states. As observed in Fig. 9, the logarithmic strain reached lasting the bulge test are not very important. Due to the geometry of the sample, it is not possible to reach a more important deformation state. For higher deformation levels, the crenels of the membranes do not allowed a 3D reconstruction of the image. Indeed, for high level of deformation some areas of the sample are not observed by the two cameras of the SDIC system, thus the reconstruction is impossible.

To highlight the stress softening, the mechanical behavior of the crenellated membrane is studied for the same pressure level for the different cycles performed during the test. Data were studied each time that the pressure level reached the values of 1.49 and 3.48 kPa during the test as highlighted in Fig. 10. The study of the different loads for the first pressure level is denoted as C_a , and four different load histories are considered ($1C_a, 2C_a, 3C_a, 4C_a$). In the same way, the study of the second pressure level is denoted as C_b ,

in this case three different load histories are considered ($1C_b, 2C_b, 3C_b, \dots$).

The results obtained for the first and the second pressure levels are illustrated and compared to FE simulation in Fig. 11. The figure highlights that the maximal in plane elongation λ_{\max} and the minimal in plane elongation λ_{\min} are approximately the same for the experimental results and for the FE simulations for the two pressure levels studied. Nevertheless, for a pressure level of 1.49 kPa (C_a), it is observed that λ_{\max} is more important for the fourth load ($4C_a$) than for the first load ($1C_a$), this is due to the Mullins effect. For λ_{\min} the behavior is identical for the different loadings since the maximal deformations are endured by direction 1 and thus the stress softening is more important for this direction.

For a pressure level of 3.48 kPa (C_b), λ_{\max} is a few superior for the third cycle ($3C_b$) than for the first loading ($1C_b$) and λ_{\min} is equal for the three different histories. As for the previous pressure level this can be explained by the Mullins effect endured by the material. Moreover, for these two pressure levels, it can be assumed that the direction of the material in the third direction, i.e. along the thickness, is modified between the different loadings (but it cannot be studied with SDIC measurements). Since the material is considered incompressible, if the material does not endured deformation due to the Mullins effect along direction 2 it supposed that the third direction endured deformations to respect the volume conservation. Nevertheless, all these simulations prove that the

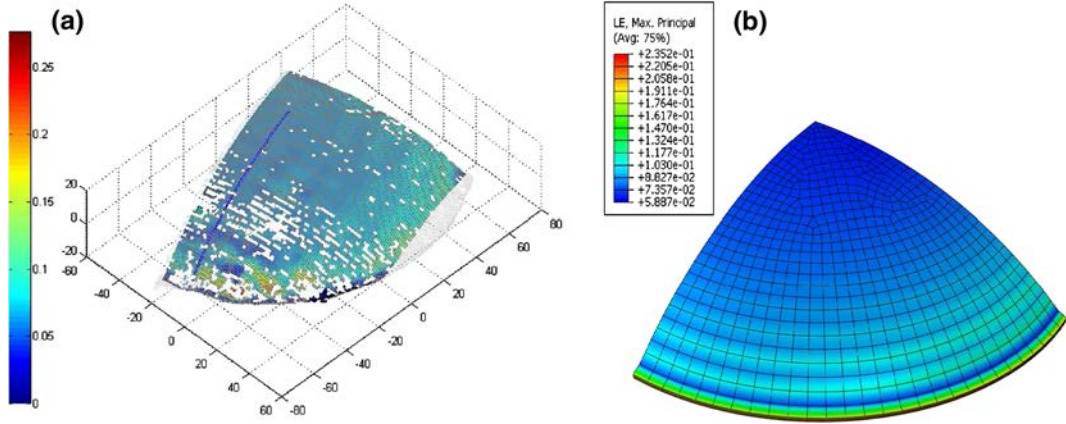


Fig. 9 Comparison of the maximal logarithmic strain field of **a** experimental tests and **b** FE simulation with coupling for bulge test, $\alpha = 45^\circ$.

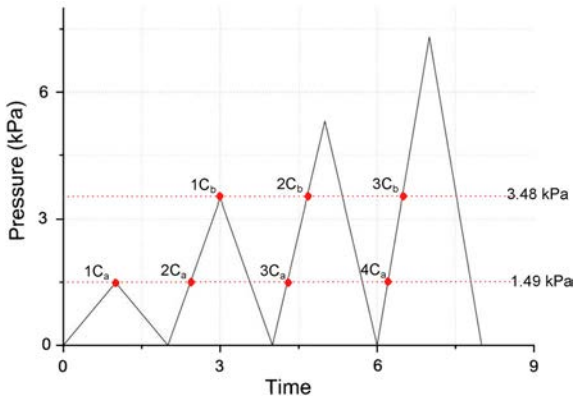


Fig. 10 Representation of the two pressure levels studied for the bulge test

equivalent model is able to well describe the strain states in a complex structure calculation i.e. for non uniaxial loading states whereas the model was developed by means of uniaxial data.

4.3 Discussion

4.3.1 About the model

For this equivalent model, it is important to note that five different mechanical parameters exist. Four of them describe the behavior of the bulk material, and are fitted on a classic tensile test sample. The fifth parameter a of Eq. (23) is the only one fitted on the crenellated membranes tensile tests.

Then, by means of a theoretical analysis the influence of each part of the constitutive equation is evaluated for the different orientations of the crenels. The behaviors of the core of the membrane, of the crenels and of the coupling term are presented in Fig. 12. For $\alpha = 0^\circ$, there is no coupling but the crenels represent 40 % of the stress. For $\alpha = 45^\circ$, there is an influence of each part of the constitutive equation, whereas for $\alpha = 90^\circ$, the influence of the crenels becomes less important. For $\alpha = 135^\circ$, the influence of the crenels becomes almost equal to zero and the coupling term tends to zero that means that the crenels can quasi be neglected. Finally for $\alpha = 180^\circ$ it is observed that the crenels and the coupling do not have any influence on the behavior of the crenellated membrane, the core of the membrane endures all.

4.3.2 Extension of the model

As exposed in literature [7], it is to note that soft tissues can be considered as architected materials. The presence of collagen [10], into the matrix of the tissues creates an initial anisotropy in this natural material. The reinforcement of fibers induces different anisotropic behavior which depends on the orientation of the fibers. The equivalent model presented here can perfectly be adapted to soft tissue. The reinforcement of fibers corresponds to the crenel and the core of the membrane corresponds to the matrix. In an aim to create biomimetic membranes that can present behavior similar to soft tissues, the use of crenellated membranes is extrapolated. Living tissues are often

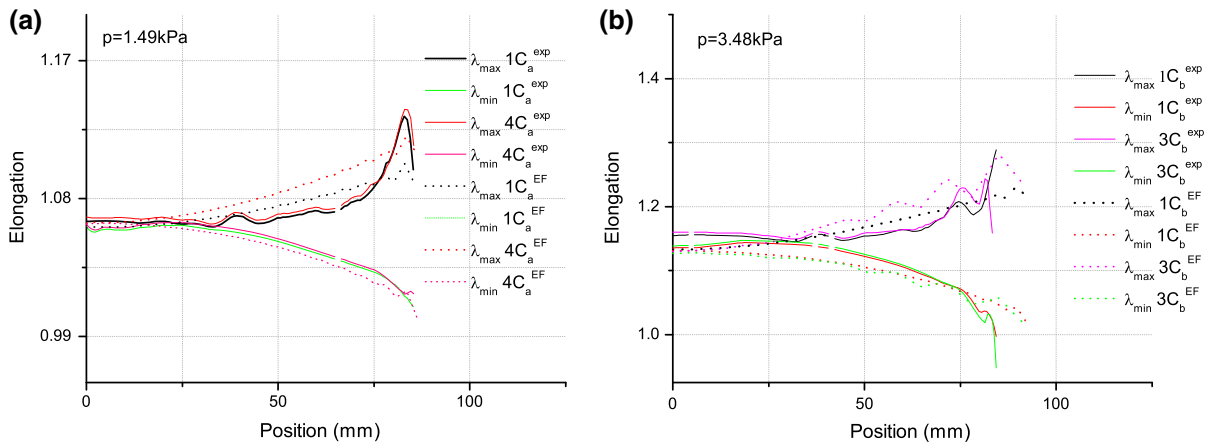


Fig. 11 Comparison of experimental tests and FE simulation with coupling for bulge test on a sample with an angle $\alpha = 45^\circ$.

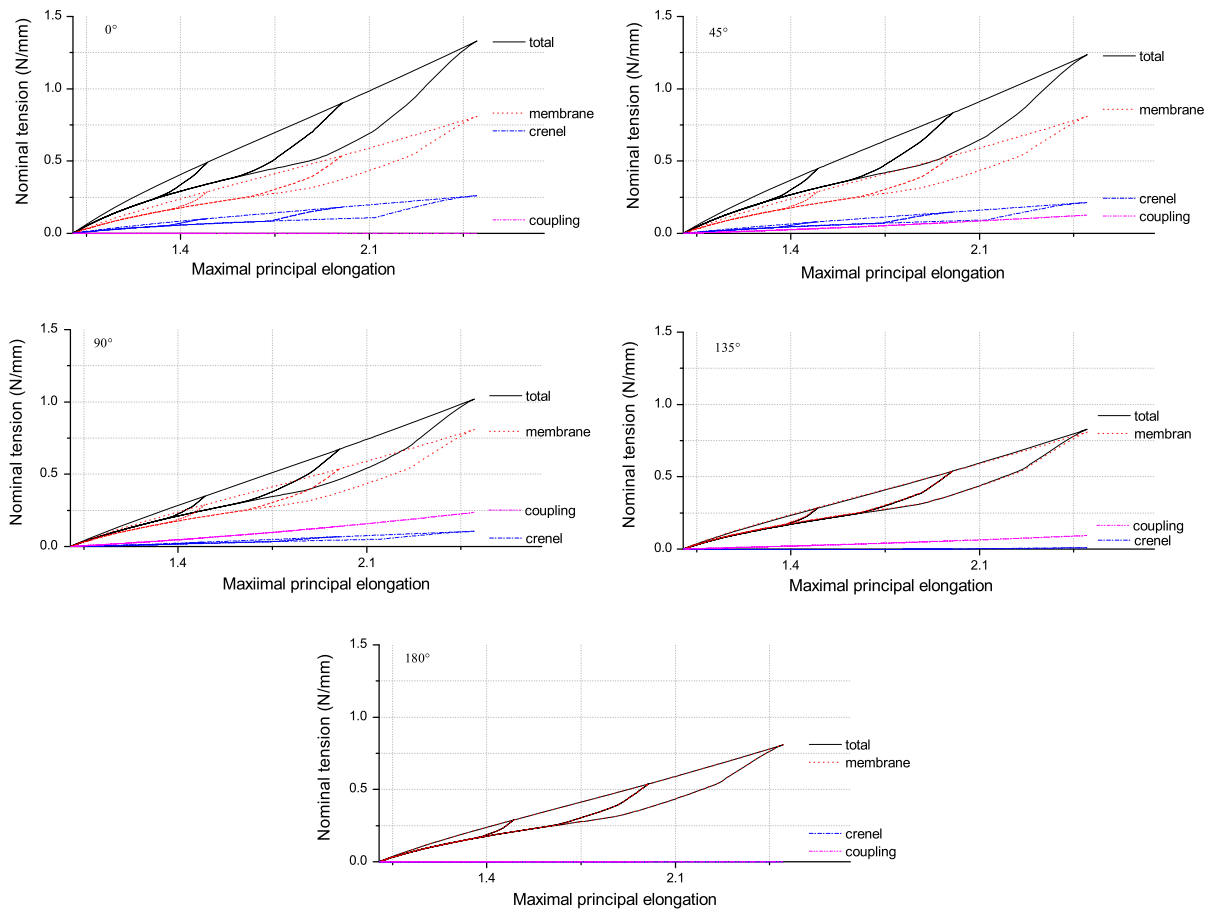


Fig. 12 Influence of each term of tension for different values of α .

characterized by a very different behavior into the two planar orthogonal directions which correspond to the tensile direction x and y for crenellated membrane (i.e.

tension for α and $180^\circ - \alpha$). In this way, Fig. 13 presents some simulations for two orientations of the crenels. The Fig. 13a presents exactly the behavior of

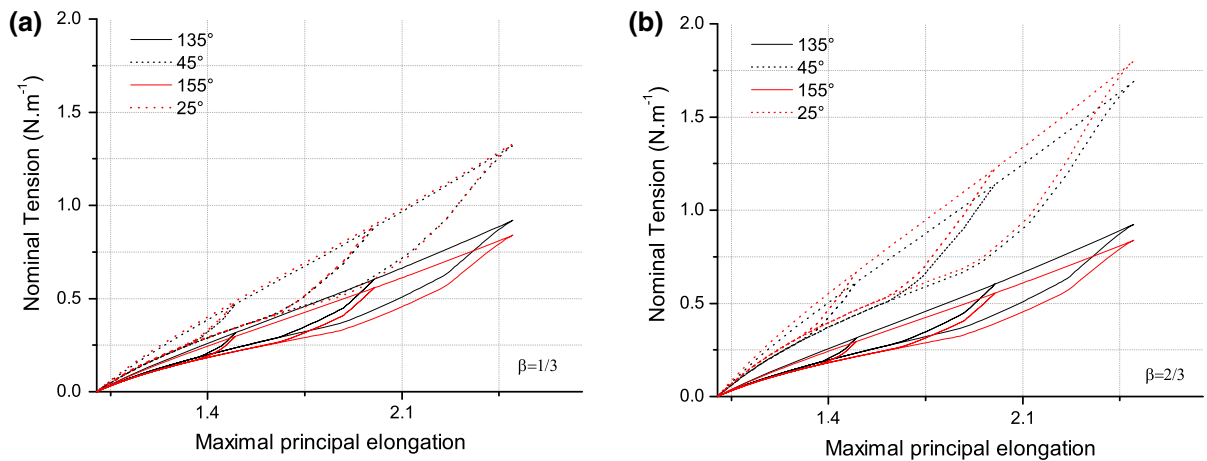


Fig. 13 Representation of the behavior of a crenellated membrane for different orientation of the crenel for $\beta = \frac{1}{3}$ (a) or for $\beta = \frac{2}{3}$ (b).

the developed membranes ($\beta = \frac{1}{3}$). The anisotropy already important presents a difference of stiffness about 30%. Moreover, Fig. 13b presents simulations for $\beta = \frac{2}{3}$, that means that the thickness of the crenels is now of 2 mm. In this case, the difference of stiffness is about 2. That means that it is possible to generate a membrane with two directions with very different mechanical behaviors. In order to come closer from soft tissues it would be necessary to use a silicone rubber that presents a more important strain hardening.

5 Conclusion

Filled silicone crenellated membranes were molded for different orientations of the crenels. According to literature, and previous works, an existing model of filled silicone rubber was used. This model was adapted to the crenels and a coupling term was developed. Thus, every parts of the crenellated membrane can be evaluated. The constitutive equation obtained was implemented into a finite element code via an Umat. Several experimental tests were performed to validate the model. It was proved that the coupling term could not be neglected during cyclic tensile tests for different orientations of the crenels. Finally, a bulge test was performed to test the robustness of the model. Even if the deformations reached are not very important for silicone rubber, it is observed that a good comparison between FE simulation and experimental results is obtained. By means

of the equivalent model, complex structures can be easily simulated with one parameter more than the material parameters of the bulk material. Finally, the crenellated architected membranes could be used in a biomimetic approach to be adapted to soft tissues.

References

1. Ashby M (2013) Designing architected materials. *Scr Mater* 68:4–7
2. Bazant ZP, Oh BH (1986) Efficient numerical integration on the surface of a sphere. *Z Angew Math Mech* 66:37–49
3. Bouaziz O (2013) Geometrically induced strain hardening. *Scr Mater* 68:28–30
4. Bouaziz O, Brechet Y, Embury JD (2008) Heterogeneous and architected materials: a possible strategy for design of structural materials. *Adv Eng Mater* 10:24–36
5. Brechet Y, Embury J (2013) Architected materials: expanding materials space. *Scr Mater* 68:1–3
6. Diani J, Brieu M, Gilormini P (2006) Observation and modeling of the anisotropic visco-hyperelastic behavior of a rubberlike material. *Int J Solids Struct* 43:3044–3056
7. Dunlop JW, Fratzl P (2013) Multilevel architectures in natural materials. *Scr Mater* 68:8–12
8. Federico S, Grillo A, Imatani S, Giaquinta G, Herzog W (2008) An energetic approach to the analysis of anisotropic hyperelastic materials. *Int J Eng Sci* 46:164–181
9. Göktepe S, Acharya SNS, Wong J, Kuhl E (2010) Computational modeling of passive myocardium. *Int J Numer Method Biomed Eng* 27:1–12
10. Holzapfel GA (2000) *Nonlinear solid mechanics—a continuum approach for engineering*. Wiley, Chichester
11. Machado G, Chagnon G, Favier D (2010) Analysis of the isotropic models of the Mullins effect based on filled silicone rubber experimental results. *Mech Mater* 42:841–851

12. Machado G, Favier D, Chagnon G (2012a) Determination of membrane stress–strain full fields of bulge tests from SDIC measurements. Theory, validation and experimental results on a silicone elastomer. *Exp Mech* 52:865–880
13. Machado G, Chagnon G, Favier D (2012b) Induced anisotropy by the Mullins effect in filled silicone rubber. *Mech Mater* 50:70–80
14. Meunier L (2011) Contribution la conception, l’expérimentation et la modélisation de membranes hyperélastiques architecturées anisotropes. Ph.D. thesis, Université de Grenoble
15. Mooney M (1940) A theory of large elastic deformation. *J Appl Phys* 11:582–592
16. Mullins L (1948) Effect of stretching on the properties of rubber. *Rubber Chem. Technol.* 21:281–300
17. Natali AN, Carniel EL, Gregersen H (2009) Biomechanical behaviour of oesophageal tissues: material and structural configuration, experimental data and constitutive analysis. *Med Eng Phys.* 31:1056–1062
18. Nerurkar NL, Mauck RL, Elliott DM (2011) Modeling interlamellar interactions in angle-ply biologic laminates for annulus fibrosus tissue engineering. *Biomech Model Mechanobiol* 10:973–984
19. Rebouah M, Machado G, Chagnon G, Favier D (2013) Anisotropic Mullins stress softening of a deformed silicone holey plate. *Mech Res Commun* 49:36–43
20. Reese S, Raible T, Wriggers P (2001) Finite element modelling of orthotropic material behaviour in pneumatic membranes. *Int J Solids Struct* 38:9525–9544
21. Rey T, Chagnon G, Le Cam J-B, Favier D (2013) Influence of the temperature on the mechanical behavior of unfilled and filled silicone rubbers above crystallization temperature. *Polym Test* 32:492–501
22. Spencer AJM (1971) Theory of invariants. *Contin Phys* 1:239–352